Available online at www.eccomasproceedia.org
Eccomas Proceedia COMPDYN (2021) 4983-4992

ECCOMAS
Proceedia

COMPDYN 2021
8th ECCOMAS Thematic Conference on
Computational Methods in Structural Dynamics and Earthquake Engineering
M. Papadrakakis, M. Fragiadakis (eds.)
Streamed from Athens, Greece, 28 - 30 June 2021

COUPLED ANALYSIS OF SEISMIC PILE-TENDON-PLATFORM INTERACTION IN LIQUEFIABLE SEABED

Yannis K. Chaloulos[1], Yannis Z. Tsiapas[1], George D. Bouckovalas[1] and Konstantinos N. Bazaios[1]

[1] National Technical University of Athens
Iroon Politexniou 9, 15780 Zografou, Attica, Greece
e-mail: y.chaloulos@gmail.com, ioannis.tsiapas@gmail.com, gbouck@central.ntua.gr, kon_bazeos@hotmail.com

Abstract

The paper presents numerical analyses of a pile supported Tension Leg Platform wind turbine, during seismic loading and seabed liquefaction, taking consistently into account the pile-tendon-platform interaction. The emphasis is on the system response when liquefaction in the subsoil is extensive, leading to degradation of the pseudo-static factors of safety against pullout failure of the pile well below unity. It is shown that the pile resistance to pullout failure decreases drastically during shaking, but fully recovers during the following dissipation of earthquake-induced excess pore pressures and even exceeds the initial (pre-shaking) resistance value. Pile head displacements develop steadily during shaking and the following excess pore water pressure dissipation phase, but only during the limited time period when the static pullout factor of safety of the pile remains less than unity. Due to the very high tensional stiffness of the tendons, relative to the buoyancy stiffness of the platform considered in this study, the pile head pullout is mostly transmitted to the platform, with only a very small part corresponding to reduction of tendon elongation. As a result, the potential loss of buoy stability and tendon pretension may prove detrimental, but they are recoverable following a strong seismic event, as is unlikely to threaten the short-term safety of the platform.

Keywords: TLP Platform, Liquefaction, Numerical Analysis, Offshore pile foundation.

ISSN:2623-3347
Peer-review under responsibility of the organizing committee of COMPDYN 2021.
doi:10.7712/120121.8843.18540

1 INTRODUCTION

Compared to bottom-fixed support platforms (e.g. gravity base, tripod, monopile and "jacket" supporting structures), the cost of Tension Leg Platforms (TLPs) depends on depth only for the station keeping component and becomes competitive for relatively large water depths, beyond about 80 m (e.g. Big Foot TLP, Magnolia TLP, Ursa TLP etc.). In addition to the lower construction cost, the TLP concept is also appealing for high seismicity areas (e.g. Italy, East Mediterranean, California, China, Japan), as it is rather insensitive to seismic actions, especially when the pile foundation response is considered along with the tendon-buoy dynamic model (e.g. [1-4]).

Nevertheless, it should be noted that the previous findings apply to seismically stable soil and foundation conditions, but they are still under consideration for liquefiable sand and silt seafloor soil profiles, where seismic shaking may lead to excess pore pressure buildup and partial or total loss of the pile foundation capacity to sustain the pretension of the tendons [5]. The static design of pile foundations is described with sufficient detail in a number of design guidelines [6-7]. However, available guidance on the seismic design of TLP foundations is limited and practically non-existent for earthquake-induced liquefaction in the foundation soil.

In view of the above objective limitations, the paper presents numerical analyses of a TLP supported wind turbine during seismic loading and seabed liquefaction, taking consistently into account the pile-tendon-platform interaction. The emphasis is on the system response when liquefaction in the subsoil is extensive, leading to degradation of the pseudo static factors of safety against pullout failure of the pile well below unity. For this purpose, it was assumed that the liquefiable soil deposit extends along the entire pile length, instead of forming one or more layers of limited thickness.

2 NUMERICAL MODELLING

2.1 The POSEIDON Model Floating Platform

The basic data for the numerical analyses are derived from the POSEIDON model TLP (Figure 1a), which was conceptually designed and analyzed for combined wind and wave energy exploitation in Mediterranean Sea conditions [8]. In particular, the system consists of a triangular platform supported by cylindrical floaters with a 5 MW wind turbine mounted at deck's center and three cylindrical oscillating water column (OWC) devices at its corners. The spacing between each OWC is 50 m. In the center of the platform, a cylindrical solid body is arranged to support the wind turbine. When positioned and stabilized, the draught of the platform is 20 m and the tower of the wind turbine is cantilevered at an elevation of 10 m above sea water level (SWL), at the top of the main column of the floating platform.

The floating structure is held in position by a Tension Leg Platform mooring system, which consists of three steel tendons, anchored at the seabed. The tendons are symmetrically placed and mounted at the base of the offset columns, i.e. at a depth of 20 m below the SWL. The diameter of each tendon is 0.130 m, while its length varies in each examined location. In all cases, the pretension load of each tendon is equal to $F_o = 10800$ kN. This load is transferred to the foundation system of the platform, which consists of a single driven open-ended steel pile under each tendon. The mass, including ballast, of the floating platform is 2183.6 t. The equivalent, in terms of buoyancy force, cross-section area of the platform is 298.53 m^2.

The pilot foundation design of the POSEIDON platform was conducted parametrically for two installation locations in the Aegean Sea, assuming typical soil profiles that cover the basic soil types commonly encountered in offshore sites. Of interest for the present study is

the case of the non-cohesive seabed with medium density sand of relative density $D_r = 50\,\%$, which is susceptible to earthquake-induced liquefaction.

The foundation piles were properly designed to withstand the combined static and cyclic axial loads applied during the normal and extreme environmental design conditions [9]. In more detail, the static loads come from the pretension of the steel tendons (i.e. $F_o = 10800\,\text{kN}$), while the cyclic loads are due to sea waves during a storm. The geometry of the pile (length and diameter) was defined in order to ensure a that the factor of safety against static pullout of the pile is greater than 2.0 for normal environmental conditions and greater than 1.50 for extreme environmental conditions [6-7]. This led to the selection of a steel pipe pile of $L = 55\,\text{m}$ length and $D = 2.5\,\text{m}$ outer diameter.

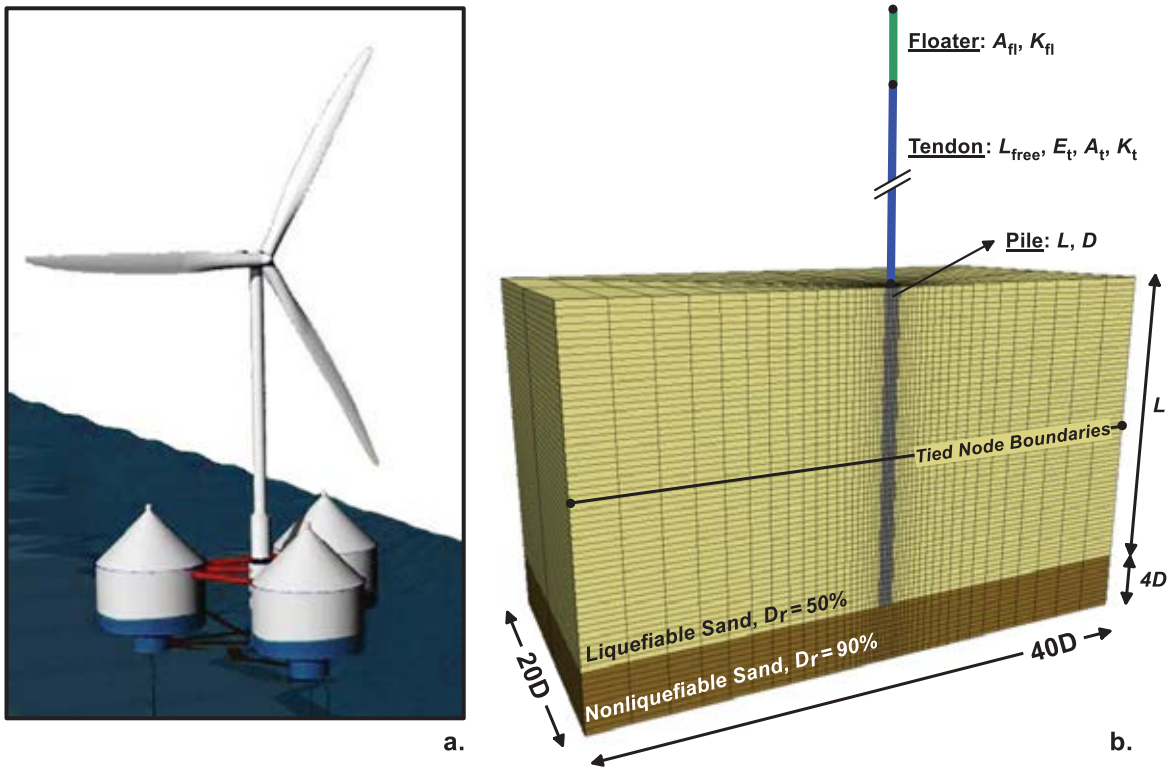

Figure 1: (a) Illustrative presentation of the POSEIDON floating TLP [10], (b) The 3D numerical model of the pile-tendon-floater system.

2.2 The 3D Numerical Model

The problem is analyzed numerically by means of 3D coupled dynamic analyses with the finite difference code FLAC3D v6.0 [11]. The specific code employs an explicit scheme for the integration of the equations of motion which is more efficient for highly nonlinear problems like the one analyzed herein, while it allows for coupling between water flow and dynamic loading.

The 3D mesh built to simulate the problem is shown in Figure 1b. A pile of length L and diameter D is installed in a liquefiable uniform layer of Nevada Sand of relative density D_r and permeability k. As the OWCs are at large distance apart, i.e 50 m, each pile and tendon support is simulated independently. The liquefiable sand layer extends to the depth of the pile tip, followed in depth by a much denser non-liquefiable sand layer of thickness $4D$.

The pile supports a floater, defined in terms of its cross-sectional area A_{fl}, through a pretensioned tendon of free length (before pretension) L_{free}, cross-sectional area A_t and Young's modulus E_t. The floater-tendon system can be adequately represented by two serially connect-

ed springs [12] which are simulated herein by two sets of cable elements. The properties of the cables (length, cross-sectional area and Young's modulus) are properly calibrated to provide the axial stiffness of the tendon K_t (i.e. the tendon's resistance against unit tensile displacement) and the axial stiffness of the floater K_{fl} (i.e. the floater's resistance against unit downward displacement), computed as:

$$K_t = \frac{E_t A_t}{L_{free}} \tag{1}$$

and

$$K_{fl} = A_{fl} \cdot \gamma_w \tag{2}$$

During static uplift loading of the pile, the base of the model is fixed in all three directions and vertical hinges are applied on the vertical boundaries. During seismic shaking the hinges at the lateral boundaries are replaced with "tied-nodes" which impose the same boundary displacements at grid-points of the same elevation, replicating free field conditions, while a harmonic motion of amplitude a_{max}, period T and N cycles is directly applied at the base assuming rigid bedrock conditions. The in-plane and out-of-plane width of the mesh is 40D and 20D respectively. The thickness of each zone is 1.0m, while the width is approximately equal to 0.2D next to the pile and gradually increases to about 2.7D at the lateral boundaries.

The highly nonlinear response of the liquefiable sand is simulated with NTUA-Sand [13-14] implemented in FLAC3D as a C++ plug-in constitutive model. NTUA-Sand is also used to simulate the response of the dense sand layer below the pile tip, while the pile is simulated through elastic solid elements with the axial stiffness and the unit per length weight of a hollow steel pile with diameter $D = 2.5$ m and wall thickness $t = 31.35$ mm.

A key aspect of the numerical methodology is the accurate simulation of the pile-soil interface, as the pile-soil relative slip, as well as the pullout capacity of the pile are both related directly to the strength characteristics and the radial stresses of that interface. Following a trial-and-error approach [15], it was finally decided to install six sets of interface elements, one for each set of zones that encircle the pile. Large values are assigned to the elastic stiffnesses of the interface to ensure that no interface straining occurs before yield. The tensile strength and the shearing cohesion of the interface are set to zero, while an interface friction angle δ is adopted and properly calibrated based on relevant guidelines

2.3 Numerical Solution Sequence

The seismic response analysis of the pile-tendon-floater system is performed in two stages. Initially, the pretension force $F_o = 10800$ kN is applied statically at the structural node corresponding to the top of the floater. In the sequel, the displacement of that node is constrained, and the input seismic motion is applied at the base of the model. The analysis continues beyond the end-of-shaking, until excess pore pressures are fully dissipated. During this second stage, the displacements of the pile head and the floater are continuously monitored, along with the loss of tendon pretension and floater buoyancy. Still, to shed light on the mechanisms that control the system response, it is also necessary to monitor the variation with time, during shaking and following excess pore water pressure dissipation, of the degraded pullout capacity of the pile.

When numerically performed, the latter may extend the computational effort enormously, as it is not part of the main seismic response analysis, but it has to be performed independently at regular time intervals, based on the ever current stress state around the pile. For this reason, the static pullout capacity of the pile was computed analytically, according to the API [7]

and DNV [6] recommendations in connection with the liquefaction-affected radial stresses at the pile-soil interface predicted during the second stage of the seismic response analyses. This semi-analytical methodology has been implemented in the numerical analysis through a user-defined subroutine, written in FLAC3D's inbuilt programming language FISH, to provide the continuous with time variation of the pile capacity to sustain the tendon pretension load.

3 LIQUEFACTION EFFECTS ON PILE-TENDON-FLOATER RESPONSE

3.1 Input data and assumptions

The basic analysis presented herein is performed for 120 m water depth, assuming that the relative density of the liquefiable layer is $D_r = 50\,\%$ and that of the underlying non-liquefiable sand is $D_r = 90\,\%$. The permeability is set equal to $k = 6.6 \times 10^{-4}$ m/s for both layers corresponding to a clean sand [16]. The single tendon-pile support considered in the analysis is attached to a floater with equivalent cross-section area $A_{fl} = 99.51\,m^2$ (i.e. 1/3 of the total), while the free length of the tendon is $L_{free} = 100$ m, the associated cross section area is $A_t = 0.01327\,m^2$ and the modulus of elasticity is $E_t = 200$ GPa. According to Eqs. **Error! Reference source not found.** and **Error! Reference source not found.**, the preceding values lead to an axial stiffness $K_t = 62800$ kN/m and $K_{fl} = 995$ kN/m for the tendon and the floater respectively. The input seismic motion consists of $N = 15$ uniform acceleration cycles (corresponding to an $M_w = 7.5$ earthquake) with amplitude $a_{max} = 0.24$ g and period $T = 0.5$ sec.

3.2 Pile response

Figure 2 summarizes the response of the pile-tendon-floater system. More specifically, Figure 2a presents time-histories of the pile's pullout capacity Q_{ult} and the tendon's force F (black and red line respectively) both during and after the end of shaking until full excess pore pressure dissipation. Similarly, Figure 2b presents the factor of safety against pullout of the pile $FS = Q_{ult}/F$ as well as the Stability Safety Factor $FS_{st} = U/W_{fl}$ (U is the total buoyancy force and W_{fl} is the weight of the floater), while Figure 2c shows the uplift displacement of the pile head and the floater. To further verify the semi-analytical procedure for the estimation of Q_{ult}, during and after shaking, a set of undrained numerical analyses is performed at selected time instances in order to compute Q_{ult} and is compared with the analytical estimates. The results of these analyses are shown on Figure 2a with the cyan bullets.

Based on the above observations the following critical time instances can be identified:

- Point A ($t_A = 3.5$ sec): The factor of safety drops below 1.0 for the first time.
- Point B ($t_B = 8.0$ sec): At the end of shaking Q_{ult} reaches a local minimum practically equal to the buoyant weight of the pile.
- Point C ($t_C = 36.5$ sec): The Factor of Safety becomes again larger than unity.
- Point D ($t_D = 250$ sec): At the end of consolidation the post-shaking pullout capacity stabilizes to a value that is approximately 38 % larger than the initial.

The evolution of the pullout factor of safety is the key factor determining the accumulation of pile displacements. More specifically, as shown on Figure 2c, pile displacements are limited as long as the factor of safety remains greater than 1.0 (up to Point A) and do not exceed 5 - 6 cm. However, as the FS becomes and remains lower than unity (between points A and C) the rate of displacement accumulation increases substantially leading to uplift displacements that increase linearly with time. It is noteworthy that at the end of shaking only a fraction of the total pullout displacement has accumulated. Namely, at the end of shaking (Point B) dis-

placements are approximately equal to 30 cm, and at the end of the failure stage (Point C) they are equal to 85 cm. Afterwards (between points C and D), as the factor of safety becomes again larger than unity, displacement accumulation practically ceases and the pile stabilizes. The above observations suggest that the accumulation of pile pullout displacements is primarily influenced by the duration of the failure stage (t_A - t_C in Figure 2b) and may thus increase considerably when the excess pore water pressure dissipation is delayed (e.g. for silty sand seabed with lower permeability coefficient).

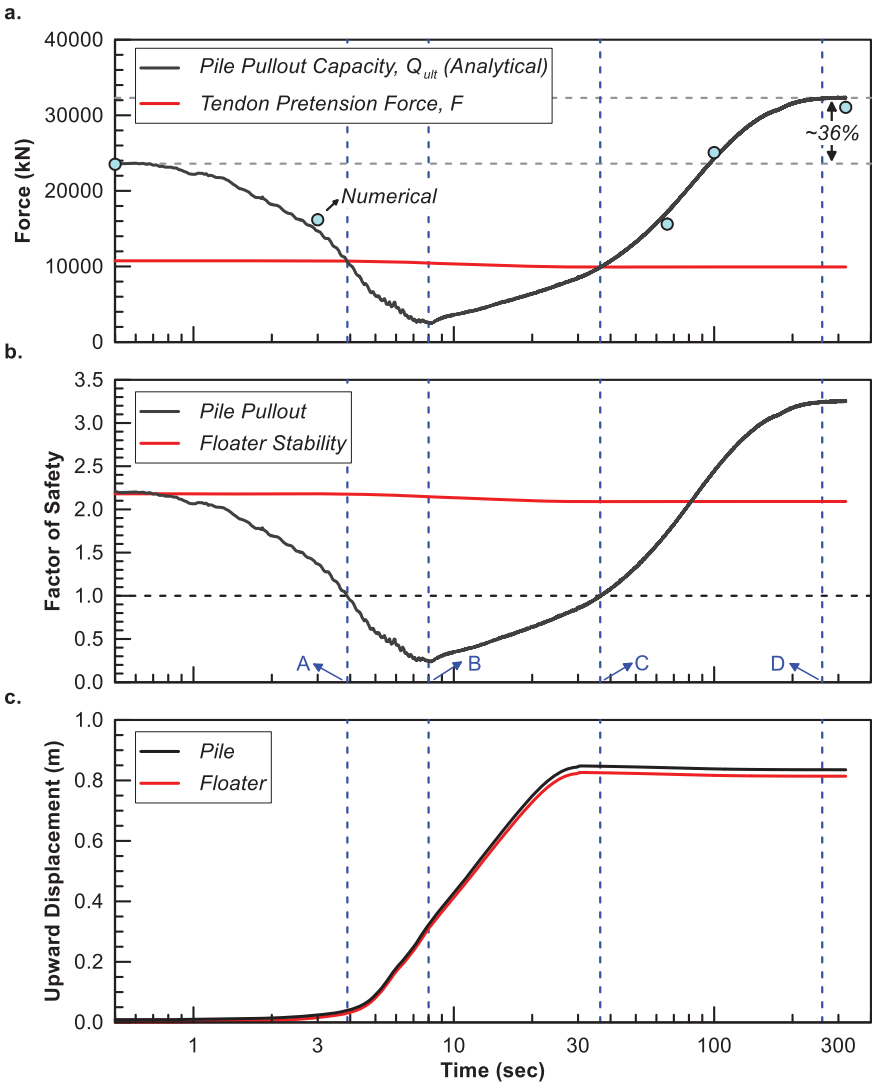

Figure 2: (a) Pile pullout capacity and tendon pretension force, (b) Pullout and Stability Factor of Safety (*FS* and FS_{st}), (c) Pile head uplift time-histories.

3.3 Soil Response

The patterns described in the previous section regarding the pullout capacity of the pile are directly associated with excess pore pressure generation and soil liquefaction. Figure 3 presents time-histories of excess pore pressure ratio r_u, defined as the ratio of the excess pore pressures Δu over the initial effective vertical stress $\sigma'_{v,o}$ (i.e. $r_u = \Delta u / \sigma'_{v,o}$), at depths $z = 1$, 10 and 40 m below ground surface both at the free field and next to the pile.

Focusing first on the co-seismic response ($t = 0$ - 8 sec), the figure shows that complete liquefaction ($r_u = 0.9$ - 1.0) takes place almost in the entire soil mass with the exception of the ar-

ea around the pile head where the excess pore pressure ratio stabilizes at a peak value of $r_u \approx 0.5\text{-}0.6$ (Figure 3). This non-liquefied zone is more clearly illustrated on Figure 4a which shows contours of r_u at the end of shaking. It has an inverted-cone shape and extends to a depth of about 4 - 5 m (1.6 - 2.0 D). Post-seismically ($t > 8$ sec), excess pore pressures dissipate primarily towards the ground surface as evidenced by the fact that excess pore pressures at large depths dissipate earlier. Furthermore, this upward flow towards areas of lower hydraulic head, causes the pore pressures near the pile head, where the soil hasn't fully liquefied, to notably increase before they also start to dissipate.

It is interesting to observe the correlation between the generation of excess pore pressures and the degradation of the pile's pullout capacity. Namely, as shown in Figure 2b, the factor of safety drops below unity at $t \approx 3.5$ sec, which, according to Figure 3, coincides with the moment when significant excess pore pressures ($r_u > 0.6$) have started to develop in the soil. Furthermore, the ultimate pullout capacity Q_{ult} and the factor of safety FS reach a local minimum at the end of shaking, when the majority of the soil is liquefied (Figure 4a). Finally, as shown on Figure 4b, at $t \approx 36.5$ sec the dissipation process has progressed significantly, the soil has regained a considerable amount of its shear strength, and thus the factor of safety becomes again larger than unity.

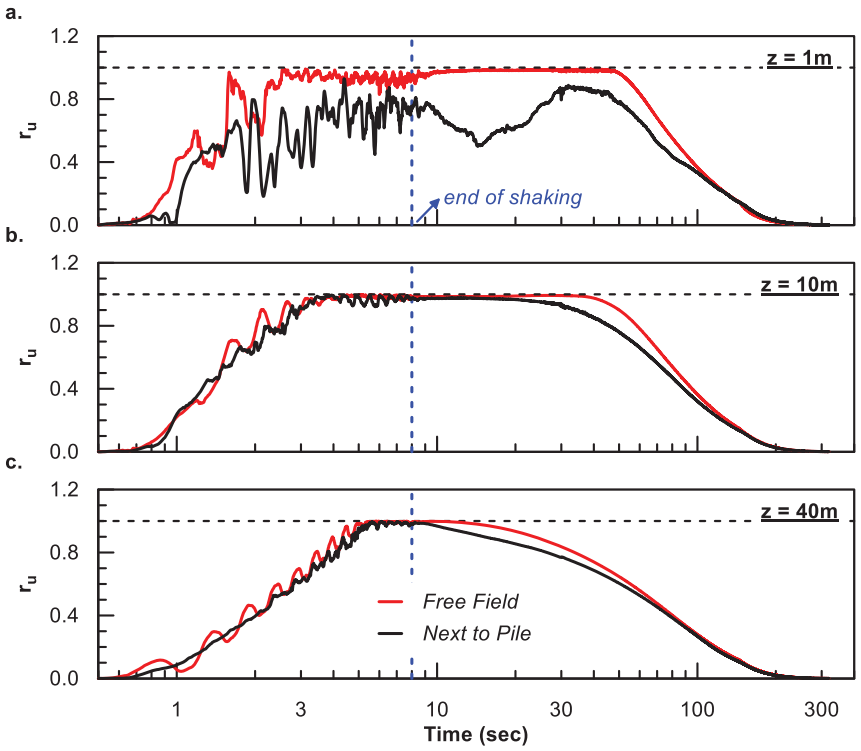

Figure 3: Excess pore pressure ratio (r_u) time-histories at the free field and next to the pile at various elevations.

3.4 Tendon & floater response

Pullout of the pile causes both the floater to move upwards as well as the tendon's elongation to decrease subsequently decreasing the pretension force. For the platform examined herein, Figure 2c presents the evolution with time of the upward displacement of the floater (red line) compared to that of the pile head (black line). As shown on this figure, the displacement of the floater resembles that of the pile head. Initially the displacement is very limited (up to Point A), while, afterwards, it increases linearly with time until the end of the failure phase (Point C). Finally, the floater stabilizes to an upward displacement of about

82 cm, approximately 3 cm less than that of the pile head. It is thus observed that the pile head displacement is almost entirely (by approximately 96 - 97 %) transmitted to the floater, while only a small portion (~ 3 - 4 %) causes the length of the tendon to decrease.

As a result, the tension force of the tendon is only marginally reduced by 7.8 %, from its initial value $F_o = 10800$ kN to approximately $F = 9950$ kN (Figure 2c). Subsequently the stability safety factor of the floater decreases by 6.2 %, from 2.25 to 2.11 (Figure 2b). It should be noted that the system studied herein employs a relatively short tendon (due to the shallow seabed) with high tensional stiffness. For larger water depths and less stiff tendons, the percentage of pile head pullout that is transferred to the floater will substantially decrease, leading to higher loss of pretension platform stability.

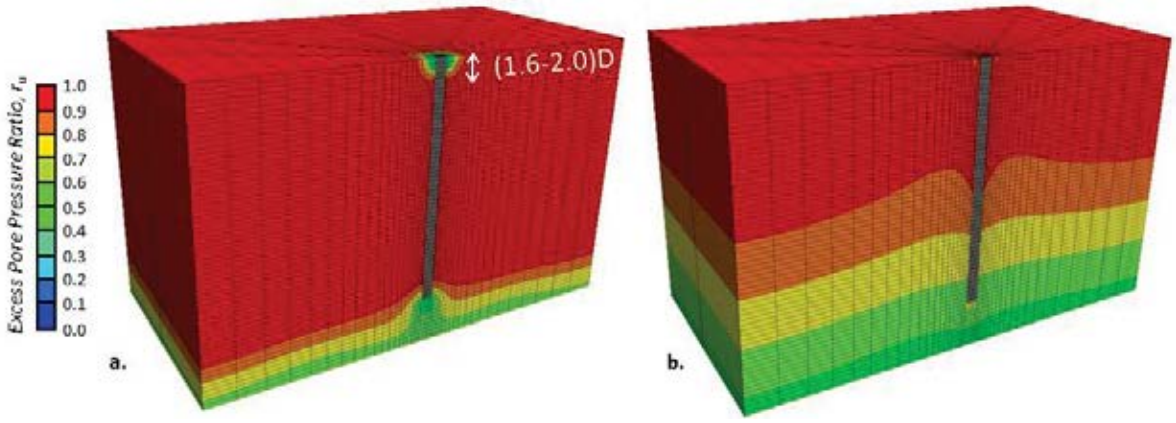

Figure 4: Excess pore pressure ratio r_u contours (a) at the end of shaking and (b) at $t = t_c$ when FS becomes greater than 1.0 post-seismically.

4 CONCLUSIONS

In summary, the following findings emerged from the study presented in this paper, with regard to seismic liquefaction effects on TLP foundation-tendon-buoy systems:

(a) Upon complete free field liquefaction, the excess pore pressure ratio becomes approximately equal to unity ($r_u = 0.9 - 1.0$) along almost the entire pile length. As a result, the skin friction resistance of the pile is drastically reduced during shaking and it is almost eliminated when free field liquefaction extends over the entire pile length. At that stage, the main force resisting the pretension of the tendons is the buoyant weight of the pile.

(b) The pile resistance to pullout failure increases with dissipation of the excess pore pressures created during shaking, while the associated factor of safety becomes gradually larger than unity, mainly due to the increase of the total radial soil stresses at the pile-soil interface caused during shaking but also to the loss of tendon pretension. For the analyses of this study, the final value of the ultimate resistance exceeds the initial static design by about 38 %, while the corresponding factors of safety increase by approximately 48 %.

(c) Pile head displacements develop essentially in the time period, during and after shaking, when the factor of safety against static pullout of the pile becomes less than unity (i.e. at failure conditions) and may thus increase considerably when the excess pore water pressure dissipation is delayed (e.g. for silty sand seabed with lower permeability coefficient). The displacements are insignificant before and after that time period, when the factor of safety remained larger than unity.

(d) Due to the very high tensional stiffness of the tendons considered herein, relative to the buoyancy stiffness of the platform, the pile head pullout was almost entirely (96-97%) transmitted to the platform with only a very small percentage (3-4%) corresponding to the reduction of tendon elongation. For larger water depths and less stiff tendons, the percentage of pile head pullout that is transferred to the floater may decrease substantially, leading to higher loss of pretension and platform stability.

(e) Despite the catastrophic per se effects of liquefaction (loss of pile capacity and large displacements), the overall stability of the floater is not jeopardized and the computed loss of the tendon's elongation and tension force is rather small to induce slackening. In addition, the above effects are potentially recoverable as the pretension force can be restored to its initial or to an even higher value, taking also into account that the post-shaking pullout capacity of the pile has considerably increased.

5 ACKNOWLEDGEMENTS

This research is carried out/funded in the context of the project "Seismic design of offshore wind turbines: Effect of pile foundation damping and soil liquefaction" (MIS 5049428) under the call for proposals "Researchers' support with an emphasis on young researchers- 2nd Cycle". The project is co-financed by Greece and the European Union (European Social Fund-ESF) by the Operational Programme Human Resources Development, Education and Lifelong Learning 2014-2020.

REFERENCES

[1] G.-S. Liou, J. Penzien, R.W. Yeung, Response of tension-leg platforms to vertical seismic excitations. *Earthquake Engineering & Structural Dynamics*, 16(2), 157-182, 1988.

[2] K. Venkataramana, Earthquake response of tension-leg-platforms in steady currents. *Earthquake Engineering & Structural Dynamics*, 23(1), 63-74, 1994.

[3] S.Chandrasekaran, Gaurav, Offshore triangular tension leg platform earthquake motion analysis under distinctly high sea waves. *Ships & Offshore Structures*, 3(3), 173-184, 2008

[4] H. Suroor, A. Arablouei, Comparison of Coupled and Decoupled Seismic Analysis of TLP Piles. *Offshore Technology Conference*, Houston, Texas, May 6-9, 2019.

[5] A.M. Kaynia, Seismic considerations in design of offshore wind turbines. *Soil Dynamics & Earthquake Engineering*, 124, 399–407, 2019.

[6] DNV, *Design of Offshore Wind Turbine Structures; Offshore Standard*. Det Norske Veritas, 2013.

[7] API, *Geotechnical and Foundation Design Considerations, ANSI/API RP 2GEO*. American Petroleum Institute, 2014.

[8] T. Mazarakos, D. Konispoliatis, G. Katsaounis, S. Polyzos, D. Manolas, S. Voutsinas, T. Soukissian, S. Mavrakos, Numerical and experimental studies of a multi-purpose floating TLP structure for combined wind and wave energy exploitation. *Mediterranean Marine Science*, 20(4), 745, 2019.

[9] G.D. Bouckovalas, S.A. Mavrakos, K.I. Andrianopoulos, T.P. Mazarakos, *Deliverable D5.2: Design of anchor piles in silty-sandy seabed*, 2015.

[10] T.P. Mazarakos, D.N. Konispoliatis, D.I. Manolas, S.G. Voutsinas, S.A. Mavrakos, Modelling of an Offshore Multi-Purpose Floating Structure Supporting a Wind Turbine Including Second-Order Wave Loads. *11th European Wave and Tidal Energy Conference Series, 11th EWTEC*, Nantes, France, September 6-11, 2015.

[11] Itasca, *FLAC3D version 6.0*. Itasca Consulting Group Inc, 2017.

[12] Y.Z. Tsiapas, Y.K. Chaloulos, G.D. Bouckovalas, K.N. Bazaios, Performance Based Design of Tension Leg Platforms under Seismic Loading and Seabed Liquefaction: A Feasibility Study. *Soil Dynamics and Earthquake Engineering*, 2021, (under review).

[13] A.G. Papadimitriou, G.D. Bouckovalas, Plasticity model for sand under small and large cyclic strains: A multiaxial formulation. *Soil Dynamics and Earthquake Engineering*, 22(3), 191-204, 2002.

[14] K.I. Andrianopoulos, A.G. Papadimitriou, G.D. Bouckovalas, Bounding surface plasticity model for the seismic liquefaction analysis of geostructures. *Soil Dynamics and Earthquake Engineering*, 30(10), 895-911, 2010.

[15] Y.K. Chaloulos, Y.Z. Tsiapas, G.D. Bouckovalas, Seismic analysis of a model Tension Leg supported Wind Turbine under Seabed Liquefaction. *Ocean Engineering*, 2021, (under review).

[16] K. Arulmoli, K.K. Muraleetharan, M.M. Hossain, L.S. Fruth, *VELACS: verification of liquefaction analyses by centrifuge studies; Laboratory Testing Program – Soil Data Report,* Research Report, The Earth. Technology Corporation, 1992.